The Journal of Chemical Physics

RESEARCH ARTICLE | SEPTEMBER 26 2025

Bingel–Hirsch reaction on actinidofullerene U@C_{2v}(9)-C_{82}: Improved regioselectivity compared to lanthanide counterpart

Special Collection: Michele Parrinello Festschrift

Daniel Torrens ; Bei Li ; Qin Wang; Laura Abella ; Yang-Rong Yao ; Josep M. Poblet ; Ning Chen ; Antonio Rodríguez-Fortea

Check for updates

J. Chem. Phys. 163, 124307 (2025)
https://doi.org/10.1063/5.0288266

View Online Export Citation

Articles You May Be Interested In

Theoretical Study of Mechanism and Regioselectivity of 1,3-dipolar Cycloaddition of N-[methyl]-C-[5-nitro-2-furyl] Nitrilimine with Dimethyl 7-oxabicyclo[2,2,1]hepta-2,5-diene-2,3-dicarboxylate

Chin. J. Chem. Phys. (April 2010)

Research Update: A hafnium-based metal-organic framework as a catalyst for regioselective ring-opening of epoxides with a mild hydride source

APL Mater. (October 2014)

Cycloaddition chemistry of thiophene on the silicon (111)-7×7 surface

J. Chem. Phys. (August 2001)

27 October 2025 16:00:08

Webinar From Noise to Knowledge
May 13th – Register now
Zurich Instruments
Universität Konstanz

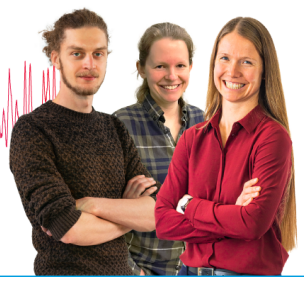

AIP Publishing

The Journal of Chemical Physics ARTICLE pubs.aip.org/aip/jcp

Bingel–Hirsch reaction on actinidofullerene U@C_{2v}(9)-C_{82}: Improved regioselectivity compared to lanthanide counterpart

Cite as: J. Chem. Phys. 163, 124307 (2025); doi: 10.1063/5.0288266
Submitted: 30 June 2025 • Accepted: 8 September 2025 •
Published Online: 26 September 2025

View Online Export Citation CrossMark

Daniel Torrens,[1] Bei Li,[2] Qin Wang,[2] Laura Abella,[1] Yang-Rong Yao,[2] Josep M. Poblet,[1] Ning Chen,[2,a)] and Antonio Rodríguez-Fortea[1,a)]

AFFILIATIONS

[1] Departament de Química Física i Inorgànica, Universitat Rovira i Virgili, Marcel lí Domingo 1, 43007 Tarragona, Spain
[2] State Key Laboratory of Radiation Medicine and Protection, College of Chemistry, Chemical Engineering and Materials Science, Soochow University, Suzhou, Jiangsu 215123, People's Republic of China

Note: This paper is part of the JCP Special Topic, Michele Parrinello Festschrift.
[a)] **Authors to whom correspondence should be addressed:** chenning@suda.edu.cn and antonio.rodriguezf@urv.cat

ABSTRACT

Actinidofullerenes constitute a family of fullerenes that exhibit different metal–cage interactions, electronic structures, and properties compared to lanthanidofullerenes. In this study, we investigate the reactivity of mono-uranofullerene U@C_{2v}(9)-C_{82} under the Bingel–Hirsch reaction and observe significantly higher regioselectivity, along with other differences in the reaction products, compared to La@C_{2v}(9)-C_{82}. Two products are obtained: a cycloadduct, which is the most abundant and has been characterized by x-ray crystallography, and a minor regioisomer that is most likely a single-bond product. Density functional theory calculations can explain the experimental structure and the formation of the two products and indicate that uranium is formally U(III) in both of them. The most abundant cycloadduct is formed under kinetic control, as found for other Bingel–Hirsch adducts, whereas the single-bond product is formed after oxidation of the anionic intermediate of the conventional Bingel–Hirsch reaction. This work is a new example of the unique reactivity and chemical properties of actinidofullerenes, which arise from their distinctive actinide–fullerene interactions.

© 2025 Author(s). All article content, except where otherwise noted, is licensed under a Creative Commons Attribution-NonCommercial 4.0 International (CC BY-NC) license (https://creativecommons.org/licenses/by-nc/4.0/). https://doi.org/10.1063/5.0288266

27 October 2025 16:00:08

I. INTRODUCTION

Endohedral metallofullerenes (EMFs) constitute a unique family of molecular nanostructures in which metal atoms or clusters are encapsulated inside the inner void of fullerene cages.[1,2] Since their discovery more than 30 years ago, they have been extensively studied due to their singular properties compared to C_{60} or other empty fullerenes, as well as their potential applications in fields ranging from biomedicine to single-molecule magnets and quantum information sciences.[3–12] A crucial feature of EMFs, which is at the origin of their different properties, is the formal charge transfer from the encapsulated metal to the carbon cage. Therefore, the electronic structure of EMFs can be easily rationalized using a simple ionic model of interaction, as for example in the mono-metallofullerene $La^{3+}@C_{82}^{3-}$ or in the prototypical nitride clusterfullerene $Sc_3N^{6+}@C_{80}^{6-}$.[13–16] Mono-metallofullerenes containing lanthanides have been known for a long time, and almost all of the lanthanides have been encapsulated in fullerene cages with relatively high yields.[1,2] More recently, actinide-containing EMFs have been synthesized in an electric arc and fully characterized.[17–21] In mono-thoriumfullerenes, formal transfer of four electrons is observed, but isomer-dependent oxidation state (III or IV) can be observed in mono-uranofullerenes, as for example in U@C_{82} isomers.[18,20] The versatility of U to be in different oxidation states when encapsulated in fullerenes was recently confirmed with the synthesis and detection of the smallest uranofullerene, U@C_{27}B, in which highly oxidized U(VI) is found at the center of the C_{27}B heterocage.[22] In diactinido or actinido–lanthanido

© Author(s) 2025

EMFs, the fullerene cage plays the role of a nanocontainer that isolates the internal guests and allows the study of the elusive actinide–actinide or actinide–lanthanide bond,[23–26] as well as the lanthanide–alkaline earth bond[5,27] and the lanthanide–lanthanide bond.[11,28] Carbide, nitride, and fluoride actinide clusterfullerenes have also been characterized.[27,29–32]

Chemical functionalization is crucial in expanding the utility of EMFs. Modifying the fullerene surface enables tuning of key properties such as electronic structure, solubility, and biocompatibility,[33–35] and can also serve as a practical and cost-effective method for EMF separation from complex mixtures.[36–38] A variety of chemical reactions have been developed to functionalize EMFs, most of which are adapted from methods originally applied to empty fullerenes. Among the most widely used are [2 + 1] cyclopropanation reactions such as the Bingel–Hirsch reaction,[39,40] [3 + 2] cycloadditions such as the Prato reaction,[41,42] and [4 + 2] Diels–Alder cycloadditions.[43–45] Other remarkable approaches include radical additions, carbene insertions, nucleophilic additions, and photochemical reactions.[46–52] These reactions typically form exohedral bonds between the fullerene cage and organic fragments, generating mono- or multi-adducts with a range of functional groups. However, unlike empty fullerenes, EMFs often display lower reactivity and more complex behavior due to the reduced molecular symmetry and the influence of the encapsulated metal species. This results in a greater number of possible reaction sites and regioisomers, making product control and purification significantly more challenging. In many cases, metal-to-cage charge transfer and specific metal–cage interactions critically influence the site and outcome of the reaction, leading to unique regioselectivity patterns not observed in empty fullerenes. Understanding these structure–reactivity relationships remains a key goal in the field, especially for actinidofullerenes, for which fewer examples of successful derivatization exist.[53,54]

Herein, we add a new example of the chemical reactivity of the mono-actinide U@C_{2v}(9)-C_{82} isomer through the Bingel–Hirsch reaction. Unexpectedly higher regioselectivity and other differences are observed compared to mono-lanthanide La@C_{2v}(9)-C_{82}. Density Functional Theory (DFT) computations can explain the formation of the two products of the reaction.

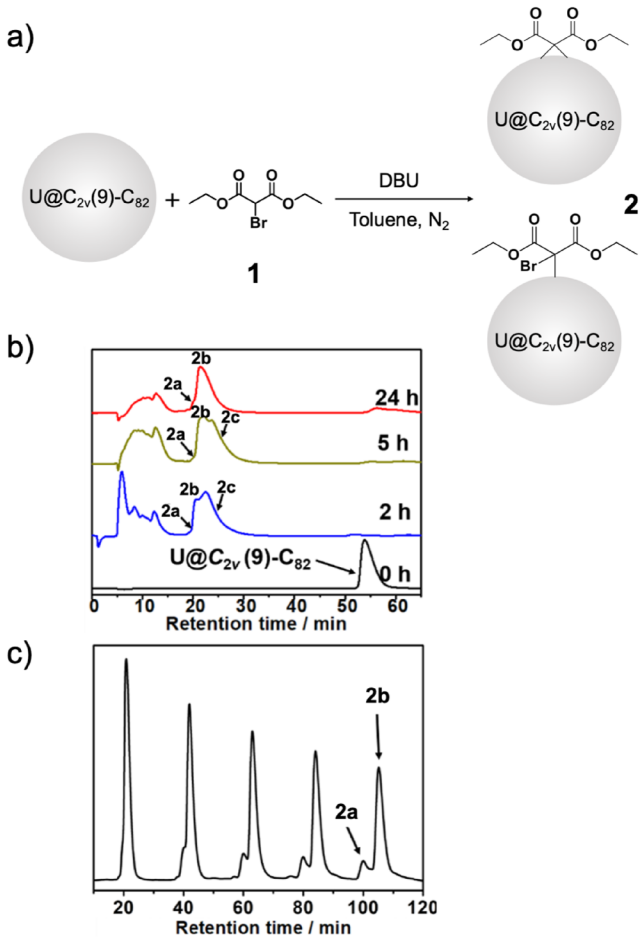

FIG. 1. (a) Scheme of the Bingel–Hirsch reaction of U@C_{2v}(9)-C_{82} with (**1**) in the presence of 1,8-diazabicyclo[5.4.0]-undec-7-ene (DBU). (b) HPLC profiles of the reaction mixture probed at different times. (c) Recycling the HPLC profile for the separation of **2a** and **2b**. HPLC conditions: Buckyprep column (10 × 250 mm^2), 4 ml/min; UV detector, λ = 310 nm.

II. RESULTS AND DISCUSSION

A. Synthesis and isolation of Bingel–Hirsch products of U@C_{2v}(9)-C_{82}

The Bingel–Hirsch reaction was carried out on U@C_{2v}(9)-C_{82} by mixing 3 mg (2.5 μmol) of U@C_{2v}(9)-C_{82} and 0.75 μl (4.4 μmol) of diethyl bromomalonate (**1**) in the presence of 0.2 μl (1.3 μmol) of 1,8-diazabicyclo[5.4.0]-undec-7-ene (DBU) in anhydrous toluene, and the mixture was stirred at room temperature under a N_2 atmosphere [Fig. 1(a)]. The results were also monitored by analytical HPLC [Fig. 1(b)]. Before the reaction, only one HPLC peak of U@C_{2v}(9)-C_{82} appeared at a retention time around 54 min. After a reaction for 2 h, the peak of U@C_{2v}(9)-C_{82} vanished completely, with mono-adduct and multi-adduct compounds appearing at 8–16 min and 18–25 min. These mono-adduct compounds were identified as mono-adducts **2a**, **2b**, and **2c**, respectively, by matrix-assisted laser desorption/ionization time-of-flight (MALDI-TOF) mass spectrometry (Figs. S1 and S2). It was apparent that isomer **2c** is unstable and transformed to isomer **2b** after 24 h, because the peak intensity of **2b** is significantly increased after 24 h. A recycling HPLC separation process was further employed to isolate these mono-adduct isomers. After the recycling process, **2a** and **2b** were successfully isolated [Fig. 1(c)]. The conversion yields of **2a** and **2b** were calculated to be ~15% and ~85%, as estimated by their HPLC peak area. **2c** was not obtained after the recycling process, suggesting that it is likely a short-lived, kinetically favorable product.

B. X-ray crystallographic study of U@C_{2v}(9)-$C_{82}C(COOC_2H_5)_2$

The molecular structure of **2b** was determined by single-crystal x-ray diffraction (XRD) analysis, and all attempts to obtain a single crystal of **2a** have failed because of the small amount of product. Black crystals of **2b** were obtained by slow evaporation of a solution of **2b** in carbon disulfide (CS_2) with *n*-hexane layered above. There are two cage orientations (0.50 occupancy each) and six disordered

27 October 2025 16:00:08

© Author(s) 2025

positions for the uranium ion, which could be described as three distinct uranium positions for each of the two cage orientations (Figs. S3 and S4).

Figure 2(a) shows the molecular structure of **2b** with the major metal site (U1) inside the cage. It is clear that a C–C bond at the [6, 6] ring junction of the original U@C_{2v}(9)-C_{82} has broken upon formation of the derivative; the C–C distance in the Bingel–Hirsch adduct U@C_{2v}(9)-$C_{82}C(COOC_2H_5)_2$ is opened to 2.221 Å. The U1 site is located over a hexagon portion of the carbon cage, with U–C distances ranging from 2.338 to 2.543 Å, similar to the values in pristine U@C_{2v}(9)-C_{82}. In addition, the U1 site is also far from the bromomalonate group, a typical observation for nucleophilic reactions, similar to what was observed for U@C_s(4)-$C_{82}C(COOC_2H_5)_2$,[54] as well as for La@C_{2v}(9)-C_{82}-$CBr(COOCH_2CH_3)_2$.[55]

C. UV–vis–NIR spectroscopic characterization and electrochemical studies

Figure 3 shows the UV–vis–NIR absorption spectra of **2a**, **2b**, and U@C_{2v}(9)-C_{82} in CS_2. Product **2b** displays the characteristic absorptions at 618 and 983 nm, which are almost identical to those of U@C_{2v}(9)-C_{82} in the NIR field, indicating a weaker impact of the addition of the bromomalonate group on the electronic structure of U@C_{2v}(9)-C_{82}. However, the absorption features of **2a** are notably different from those of the pristine U@C_{2v}(9)-C_{82}. The onset of **2a** shifts to a shorter wavelength (1308 nm), as compared with U@C_{2v}(9)-C_{82}. This finding suggests that **2a** has a larger HOMO–LUMO gap than U@C_{2v}(9)-C_{82}, and the electronic structure is different from the parent U@C_{2v}(9)-C_{82}. Therefore, we speculate that it is likely a singly bonded monoadduct, similar to those reported monoadducts of La@C_{2v}(9)-C_{82}.[55,56]

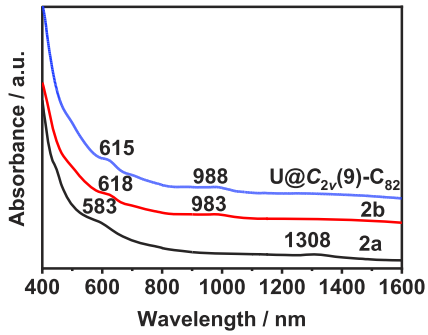

FIG. 3. UV–vis–NIR absorption spectra of **2a**, **2b**, and U@C_{2v}(9)-C_{82} in CS_2.

Figure 4 shows the cyclic voltammograms of U@C_{2v}(9)-C_{82} and U@C_{2v}(9)-$C_{82}C(COOC_2H_5)_2$ (**2b**) measured in *o*-dichlorobenzene (*o*-DCB) solution using tetrabutylammonium hexafluorophosphate as a supporting electrolyte. Table I lists the electrochemical potentials of U@C_{2v}(9)-C_{82} and **2b**. The cyclic voltammogram of **2b** presents one oxidation step and four reduction steps. The first oxidation step is reversible at 0.06 V, identical to that of U@C_{2v}(9)-C_{82} (0.06 V). For the reduction steps, the first reductive process (−0.42 V) is reversible, and the other reductive processes are irreversible. The first reduction potential of **2b** is negatively shifted by 0.06 V. Accordingly, the electrochemical gap of **2b** (0.48 V) is slightly smaller than that of U@C_{2v}(9)-C_{82} (0.54 V). The small shifts of oxidation and reduction potentials indicate that the HOMO and LUMO of **2b** likely resemble those of pristine U@C_{2v}(9)-C_{82}, as confirmed in our computational study.

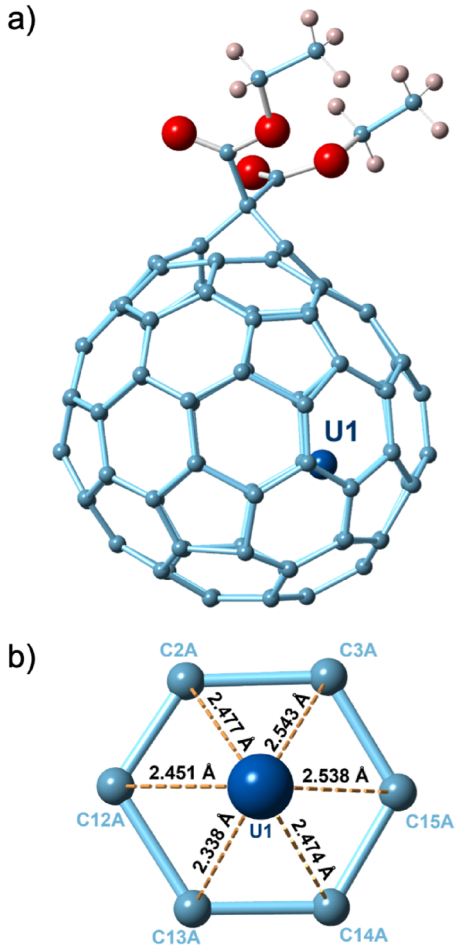

FIG. 2. (a) The molecular structure of U@C_{2v}(9)-$C_{82}C(COOC_2H_5)_2$ (**2b**). (b) The view showing the interaction of the metal ion (major U site) with the closest cage portion of **2b**.

D. Computational analysis: Structural parameters and electronic structure

The molecular structure of **2b** determined by single-crystal x-ray diffraction analysis is shown in Fig. 2, and the optimized structure at the DFT level (see Sec. IV D) is in Fig. 5(a). The Bingel–Hirsch reaction takes place in a [6, 6] bond, labeled as 1–2 [see Fig. 5(b)]. Upon the formation of the derivative, the 1–2 bond is broken with a C–C distance of 2.221 Å. This value is in very good agreement with the DFT geometry optimization (2.190 Å). The U atom is located on a corannulene motif far from the bromomalonate group with the shortest U-C_{cage} distance of 2.341 Å, almost the same as that in the pristine U@C_{2v}(9)-C_{82} cage (2.357 Å). A different position of U within the C_{2v}(9)-$C_{82}C(COOC_2H_5)_2$ cage much nearer to the malonate group was computed, obtaining a minimum with somewhat

27 October 2025 16:00:08

© Author(s) 2025

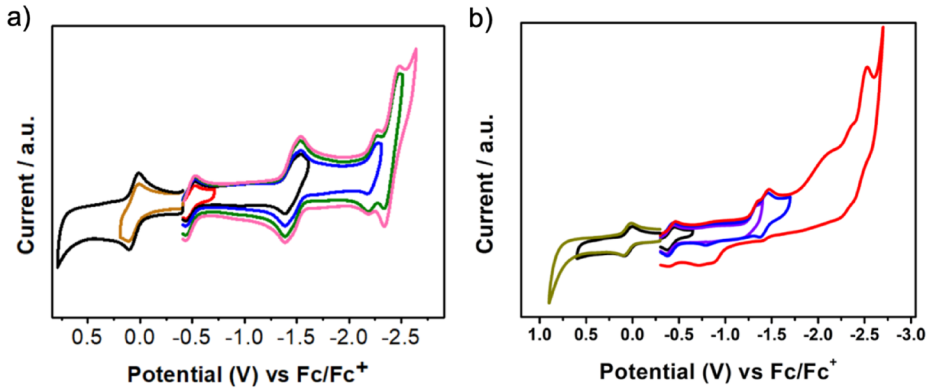

FIG. 4. Cyclic voltammogram of (a) U@C_{2v}(9)-C_{82} and (b) **2b** in o-dichlorobenzene [0.05M (n-Bu)$_4$NPF$_6$; scan rate 100 mV s^{-1} for CV].

TABLE I. Redox potentials of U@C_{2v}(9)-C_{82} and **2b**.

Compound	$E^{2+/+}$	$E^{+/0}$	$E^{0/-}$	$E^{-/2-}$	$E^{2-/3-}$	$E^{3-/4-}$	$\Delta E_{gap,ec}$/V
U@C_{2v}(9)-C_{82}	0.92[a]	0.06[b]	−0.48[b]	−1.46[b]	−2.24[a]	−2.42[a]	0.54
2b		0.06[b]	−0.42[b]	−1.35[a]	−1.46[a]	−2.53[a]	0.48

[a]Peak potential in volts (irreversible redox process).
[b]Half-wave potential in volts (reversible redox process).

larger relative energy (around 6 kcal mol^{-1}) with respect to the optimized **2b** geometry (see Fig. S5). Calculations of other positions of the uranium atom within the pristine C_{2v}(9)-C_{82} cage were also performed, showing that the U atom remains stable in that corannulene region (Fig. S6). Other positions lie higher in energy (>9 kcal mol^{-1}).

At the PBE0/TZP level, we have confirmed that U formally acts as a trivalent ion in this endohedral metallofullerene, $U^{3+}@C_{2v}(9)$-C_{82}^{3-}, consistent with previous studies.[18] Its ground spin state is a triplet, resulting in the quintet being at 3.7 kcal mol^{-1} higher in energy (Fig. 6). Therefore, unless otherwise stated, in the following study, we work with the triplet spin state configuration.

E. Reactivity of U@C_{2v}(9)-C_{82} toward the Bingel–Hirsch reaction

The Bingel–Hirsch (BH) reaction is a nucleophilic [2 + 1] cycloaddition reaction that takes place in a two-step mechanism.[57] First, deprotonated **1** reacts with the U@C_{2v}(9)-C_{82} fullerene by nucleophilic addition to form a negatively charged intermediate. In addition, second, the carbanion displaces the bromide (S_N2 reaction), and an intramolecular cyclopropane ring closure takes place.[58,59] Depending on the C–C bond where the malonate is attached, the C–C bond can appear open as a fulleroid or closed, maintaining the cyclopropane ring and the fullerene structure. In U@C_{2v}(9)-C_{82}, two mono-adduct products were obtained, the conventional BH cycloadduct **2b** (x-ray structure) and the most likely singly bonded product **2a** (based on indirect evidence). A detailed DFT analysis of the thermodynamics and kinetics of the BH reaction

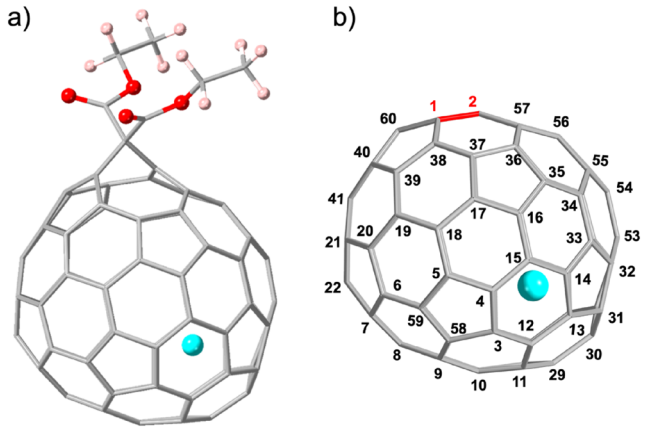

FIG. 5. (a) DFT-optimized (PBE0/TZP) geometry of **2b**. (b) Labels for the different carbon atoms of U@C_{2v}(9)-C_{82}. The C–C bond where the reaction takes place is indicated in red (1–2).

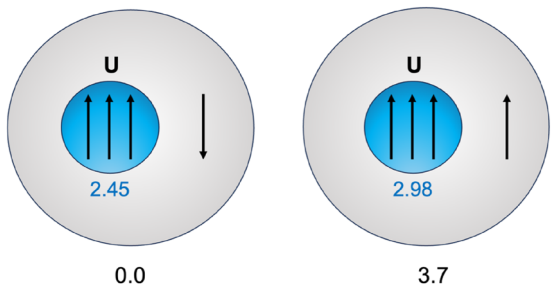

FIG. 6. Spin distribution and relative energies (in kcal mol^{-1}) for the lowest spin states of U@C_{2v}(9)-C_{82}; triplet (left) and quintet (right) spin states. Atomic Mulliken spin densities are given for each spin configuration in blue.

27 October 2025 16:00:08

© Author(s) 2025

on U@C_{2v}(9)-C_{82} was done to understand the formation of products **2b** and **2a**.

1. Formation of 2b: Analysis of products and intermediates

We first analyzed the reactivity of U@C_{2v}(9)-C_{82} to form **2b**. The addition of the bromomalonate group occurs on the 1–2 bond, which is a [6, 6] ring junction far from the U location. This is consistent with previous reaction studies of M@C_{82} (M = Gd, Y, La, and U).[54–56,60,61] Different from the recently obtained BH product of U@C_s(4)-C_{82}, in which a closed cyclopropane ring was observed, **2b** shows a [6, 6] open fulleroid structure with a C–C distance of 2.190 Å. One of the carbon atoms of the 1–2 bond (C1) is shared by three hexagonal rings (what is called a triple-hexagon junction and denoted as C-666), and the other one is shared by one pentagon and two hexagons (C-566). Interestingly, the addition to this bond does not follow the predictive aromaticity criteria for BH reactions on IPR nitride clusterfullerenes recently proposed.[59] This could be due to (i) the lower formal charge transfer compared to the case of nitride clusterfullerenes (three vs six) and (ii) the presence of the mono-actinide.

According to the lowest-energy structure of U@C_{2v}(9)-C_{82}, the BH reaction could take place on up to 66 different C–C bonds (35 if U is considered to be aligned within the C_2 axis). However, it is highly regioselective, and only one cycloadduct is obtained. The BH products with the lowest energies are provided in Table II. A complete list of all the calculated products is collected in Table S1. The adduct on bond 1–2 (experimental structure **2b**) is not the one with the lowest energy. The lowest-energy product is the adduct on bond 30–31, with the most pyramidalized carbon atoms, i.e., the most distorted region of the cage (Table S2). The adduct on bond 30–31 is also a [6, 6]-open structure with a C–C distance of 2.142 Å. In contrast to **2b**, the metal is located near the bond where the malonate is attached (Fig. S7). Then, the lowest-energy adducts are those on bonds 32–53 and 12–13 at about 1 and 3 kcal mol^{-1}, respectively (see Table II and Fig. S7). Interestingly, the BH products with the lowest energies are open-cage fulleroids, as in other cases.[62–65] Note that the experimental product **2b** is at 7.3 kcal mol^{-1} higher in energy than adduct 30–31, indicating that it is not a thermodynamic product. Test calculations at different computational levels were done for selected BH products (see Table S3) and confirmed that **2b** is not a thermodynamic product. In addition, previous studies revealed that BH reactions to EMFs usually take place under kinetic control.[58,66] Therefore, the kinetic aspects of the BH reaction on U@C_{2v}(9)-C_{82} have been analyzed by computing the different stationary points in the reaction path, intermediates (I), and transition states (TS).

Different intermediates for the addition of the malonate group on U@C_{2v}(9)-C_{82} were computed (Table III). The bromomalonate is bonded to one C atom of the C_{2v}(9)-C_{82} cage, denoted as I-X in the text. Each intermediate can lead to different conformations of the bromomalonate due to the rotation around the C_{cage}–C_{mal} bond. In the following, we distinguish them as A, B, and C, giving different products (see Fig. 7). The lowest-energy intermediates are

TABLE II. Relative energies, bond types, and C–C distances for different Bingel–Hirsch reaction products of U@C_{2v}(9)-C_{82}.[a]

Bond X–Y[b]	E_{rel}	Bond type	d (C–C)
30–31	0.0	[6, 6]-open	2.142
32–53	0.7	[6, 6]-open	2.136
12–13	3.2	[6, 6]-open	2.145
53–54	6.2	[6, 6]-closed	1.589
31–32	6.8	[5, 6]-open	2.164
30–51	7.0	[6, 6]-open	2.129
1–2 (**2b**)	7.3	[6, 6]-open	2.190
16–17	9.1	[5, 6]-closed	1.669

[a]All energies are in kcal mol^{-1} and distances in Å. Data from single point energy calculations at the PBE0/COSMO (toluene as solvent) level with the PBE0 optimized geometry.
[b]Labels for the carbon atoms according to Fig. 2(b). The experimental structure (**2b**) corresponds to the addition on bond 1–2.

TABLE III. Relative energies and Gibbs free energies (G) for selected computed intermediates (I) of the Bingel–Hirsch reaction on U@C_{2v}(9)-C_{82}.[a]

I-X[b]	Atom type	E_{rel} I	G_{rel} I	To P
I-53B	[6, 6, 6]	0.0	2.0	53–32
I-30A	[6, 6, 6]	0.5	0.0	30–51
I-30B	[6, 6, 6]	0.9	0.4	30–31
I-12	[6, 6, 6]	2.3	1.0	12–13
I-53A	[6, 6, 6]	3.5	3.4	53–52
I-1A	[5, 6, 6]	9.8	8.9	1–2
I-13B	[5, 6, 6]	10.1	10.0	12–13
I-32	[5, 6, 6]	11.4	12.0	32–53

[a]All energies are in kcal mol^{-1}. Data from single point energy calculations at the PBE0/COSMO (toluene as solvent) level with the PBE0 optimized geometry. The Gibbs free energy is calculated at room temperature. All the computed intermediates are in Table S4.
[b]The carbon atom (X) numbering is according to Fig. 2(b).

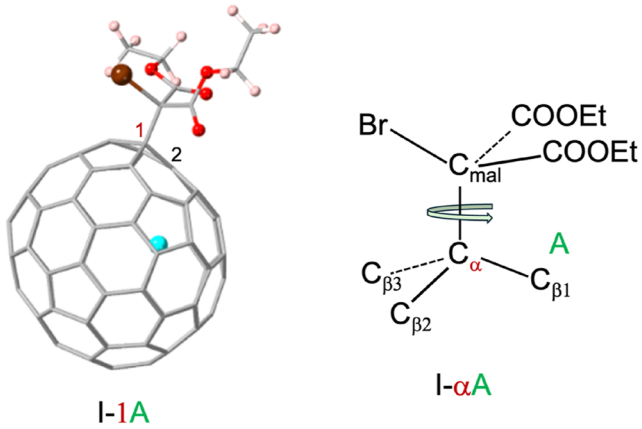

FIG. 7. Optimized structure of intermediate I-1A along with a scheme showing how the different intermediates due to rotation of the bromomalonate group around the C_α(cage)–C_{mal} are named. I-αA is the intermediate with a bond to C_α that will form the product on bond C_α–$C_{\beta1}$, with a dihedral angle Br–C_{mal}–C_α–$C_{\beta1}$ of ~180° (A). I-αB and I-αC intermediates will lead to products on bonds C_α–$C_{\beta2}$ and C_α–$C_{\beta3}$.

27 October 2025 16:00:08

© Author(s) 2025

TABLE IV. Gibbs free energies with respect to reactants for selected intermediates (I), transition states (TS), and products (P) of the BH reaction on U@C_{2v}(9)-C_{82}.[a]

I-X[b]	Atom type	ΔG I	ΔG TS	To P	G_{rel} P
I-1A	[5, 6, 6]	−14.0	−0.6	1–2	−16.6
I-30B	[6, 6, 6]	−23.6	0.7	30–31	−20.3
I-30A	[6, 6, 6]	−24.2	2.0	30–51	−20.5
I-53B	[6, 6, 6]	−24.6	3.1	53–32	−19.3
I-12	[6, 6, 6]	−18.9	6.4	13–12	−20.2

[a]Data at the M06/PCM (toluene as solvent) level with the M06 optimized geometry. The Gibbs free energy (in kcal mol^{-1}) is calculated at room temperature.
[b]The carbon atom (X) numbering is according to Fig. 2(b). The product 1–2 is the experimental product **2b**.

I-53B, I-30A, and I-30B, resulting in being close in energy (within 1 kcal mol^{-1}) at the PBE0/COSMO level (Table III). The experimental product **2b** can be obtained from either intermediate I-1 or I-2, appearing at 9.8 and 24.8 kcal mol^{-1}, respectively, higher than I-53B. Note that in I-1A, the metal atom prefers to remain not very far from the region where the bromomalonate group is attached (see Figs. 7 and S8). In the following analysis of the BH reaction path, we have focused on the lowest-energy intermediates I-53B, I-30A, I-30B, and I-12, as well as on I-1A, which leads to product **2b**.

2. Formation of 2b: Transition states and free-energy profiles

Once we made an extensive analysis of relative energies and free energies of products and intermediates, we moved to compute transition states (TSs) and free-energy profiles of the reaction. Previous works have shown that the use of the M06 functional combined with the PCM method to include solvent effects (see Sec. IV D) is an excellent combination to calculate transition states for the Bingel–Hirsch reaction in endohedral metallofullerenes.[58,66] The TSs for selected intermediates were determined and characterized (Table IV). TS-1A, which evolves to the experimental product **2b** (1–2), shows the lowest free energy, followed by TS-30B, which leads to the 30–31 product, at 1.3 kcal mol^{-1}. The transition states TS-30A (to product 30–51) and TS-53B (to product 53–32) are at 2.6 and 3.7 kcal mol^{-1} higher in free energy, respectively. TS-12 (to product 13–12) is at more than 7 kcal mol^{-1} than TS-1A. Note that, in the case of TS-1A, the U atom is positioned somewhat nearer to the carbon atom attached to the malonate compared to the 1–2 product. The corresponding free-energy profiles are displayed in Fig. 8. The present results, with TS-1A as the lowest free-energy TS, confirm that the formation of **2b** takes place under kinetic control, as in other EMFs, with a high regioselectivity. The short-lived kinetic product (**2c**) that is initially formed and completely converted to **2b** after 24 h could be a product that shares the same intermediate I-1, but with the malonate group in a different orientation, i.e., I-1B or I-1C. Product 1–38, which is 10 kcal mol^{-1} higher than product 1–2 (**2b**), could be a candidate.

3. Formation of 2a

As mentioned previously, there were no crystals obtained for product **2a**. On the basis of the different UV–vis–NIR spectrum compared to **2b**, we speculated about the possibility of a single-bond adduct as in La@C_{2v}(9)-C_{82}. Consequently, an extended DFT computational study (PBE0/COSMO) was performed in order to predict possible candidates for **2a**. 43 different single-bond products could exist in U@C_{2v}(9)-C_{82} (24 if U is considered to be aligned within the C_2 axis). We have selected the most likely carbon sites, based on pyramidalization angles and lowest-energy intermediates in the conventional BH reaction (Tables III, S2, and S4). The single-bond product is stoichiometrically identical to the intermediate in the conventional BH reaction (Sec. II E 1), but it is a neutral molecule instead of an anion. Two different spin states are possible, quartet and doublet, with different oxidation states for the internal U atom (Fig. 9). In the quartet state, the metal is U(III) with three unpaired electrons (f^3) and a closed-shell fullerene cage. In the doublet state, the metal is U(IV), with two unpaired electrons (f^2)

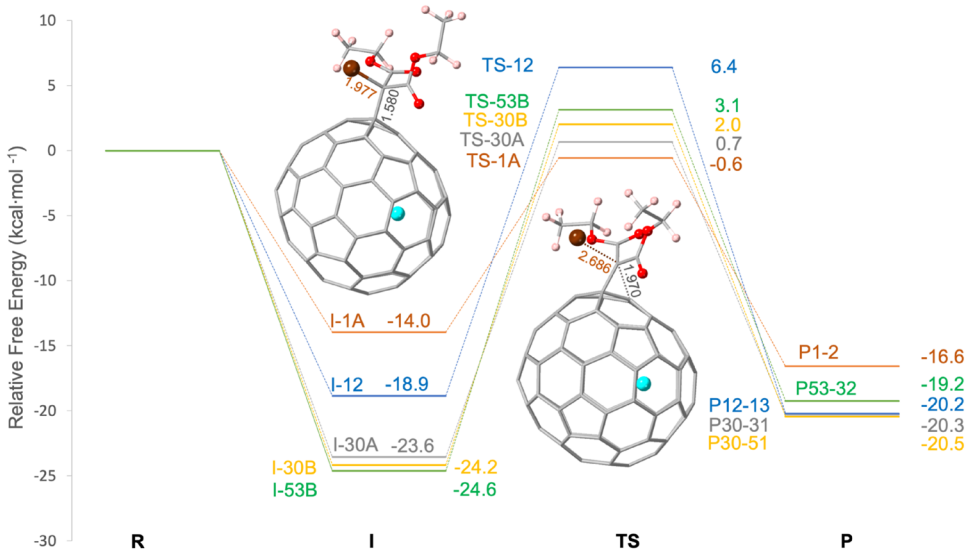

FIG. 8. Gibbs free energy profiles of the Bingel–Hirsch reaction at the M06/PCM level. Relative Gibbs free energies (in kcal mol^{-1}) with respect to reactants (R) for the intermediates (I), transition states (TS), and products (P) are indicated. Gray, yellow, green, blue, and orange lines correspond to intermediates I-30A, I-30B, I-53B, I-12, and I-1A and, consequently, their reaction pathways. The 1–2 product is the experimental structure **2b**. Bromide anion could be more stabilized in solution.

27 October 2025 16:00:08

© Author(s) 2025

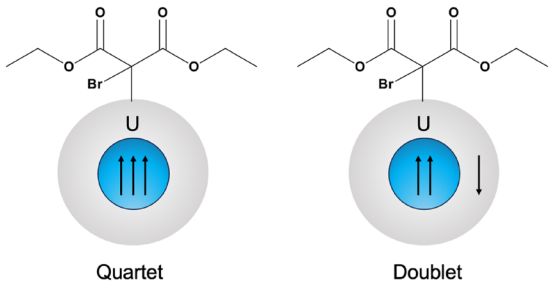

FIG. 9. Spin distribution for the quartet and doublet spin states of single-bond adducts of the BH reaction on U@C_{2v}(9)-C_{82}.

and an open-shell structure in the cage. For the products computed here, doublet states are higher in energy than quartet states. Therefore, the results in the following analysis are based on quartet spin states. Table V provides the relative energies for all the computed single-bond adducts of U@C_{2v}(9)-C_{82}. The two lowest-energy products are P-53 and P-30, both being essentially degenerate in energy. Both products show the metal near the attacked carbon site (Fig. 10). The other single-bond products are found to be at energies higher than 5 kcal mol^{-1}. Note that the adducts at either C1 or C2, i.e., P-1 and P-2, respectively, are not thermodynamically favored (see Table V).

The formation of single-bond adducts takes place after oxidation of the anionic intermediate (I-X) of the conventional BH reaction (Table III). Those intermediates with lowest free energies are likely accumulated in the experiment and, therefore, are candidates to be oxidized and form singly bonded products.[63] Upon

TABLE V. Relative energies for all the computed single-bond products of the Bingel–Hirsch reaction on U@C_{2v}(9)-C_{82}.[a]

P-X[b]	Atom type	E_{rel}
P-53	[6, 6, 6]	0.0
P-30	[6, 6, 6]	0.4
P-29	[5, 6, 6]	5.4
P-13	[5, 6, 6]	5.7
P-33	[5, 6, 6]	6.2
P-54	[5, 6, 6]	6.2
P-5	[5, 6, 6]	6.7
P-47	[5, 6, 6]	7.1
P-1	[5, 6, 6]	7.6
P-7	[5, 6, 6]	8.1
P-66	[5, 6, 6]	8.2
P-24	[5, 6, 6]	8.5
P-32	[5, 6, 6]	8.6
P-36	[5, 6, 6]	12.3
P-31	[5, 6, 6]	13.9
P-59	[5, 6, 6]	16.5
P-2	[5, 6, 6]	23.4

[a]All energies are in kcal mol^{-1}. Data at the PBE0/COSMO (toluene as solvent) level with the PBE0 optimized geometry.
[b]The carbon atom (X) numbering is according to Fig. 2(b).

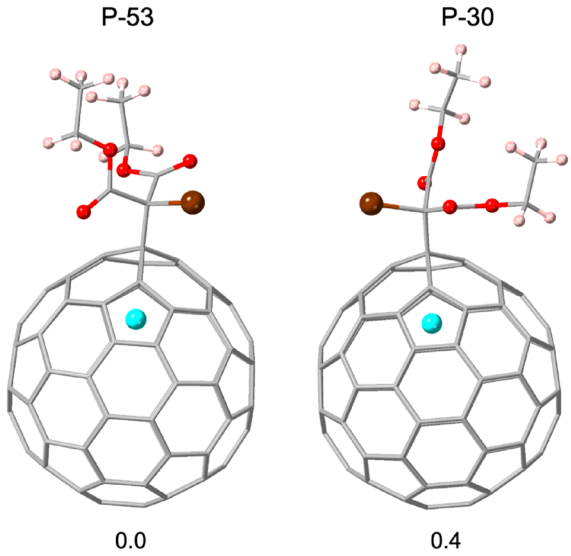

FIG. 10. Lowest-energy single-bond adducts of the BH reaction on U@C_{2v}(9)-C_{82}. Relative energies (in kcal mol^{-1}) are shown.

examining the Gibbs free-energies in toluene of the intermediates of the conventional BH process (see Table IV and Fig. 8), we propose that **2a** may be the single-bond product P-53 or P-30. The Gibbs free energies of intermediates I-53 and I-30 are the lowest ones indicating that they could be accumulated. Furthermore, Table V shows that the single-bond adduct at C-53 shows the lowest energy along with P-30.

III. CONCLUSIONS

A new example of the reactivity of an actinidofullerene is presented. U@C_{2v}-C_{82}(9) is the second actinidofullerene functionalized with the Bingel–Hirsch reaction after isomer U@C_s-C_{82}(4). Two products were obtained, **2a** and **2b**, the latter with a much higher yield. Product **2b** is characterized by UV–vis–NIR and x-ray crystallography as a cycloaddition open fulleroid product with the U atom far from the functionalized bond. No crystals were obtained for **2a**. Based on its characteristic UV–vis–NIR spectrum with a smaller onset (i.e., larger HOMO–LUMO gap) compared to **2b**, we speculate **2a** to be a single-bond adduct as found in La@C_{2v}-C_{82}(9). Although the same reaction takes place under the same conditions, there are many differences between U@C_{2v}(9)-C_{82} and La@C_{2v}(9)-C_{82}. First, U@C_{2v}(9)-C_{82} has a higher regioselectivity than La@C_{2v}(9)-C_{82}, which shows five mono-addition products. Second, U is more disordered relative to La. Finally, the product with the highest yield of U@C_{2v}(9)-C_{82} is the cycloaddition product, which is different from the most abundant single-bond addition product of La@C_{2v}(9)-C_{82}. DFT calculations can explain the formation of **2b** (x-ray structure) and **2a** (most likely a single-bond adduct), as well as the short-lived kinetic third product (**2c**). The formation of most abundant product, **2b**, is kinetically controlled, as found for other BH adducts. Single-bond adduct **2a** is formed after oxidation of the anionic intermediate of the conventional BH reaction. Moreover, the calculations show that uranium is formally

27 October 2025 16:00:08

© Author(s) 2025

U(III) in the two products. In conclusion, in the same reaction, the same carbon cage with different embedded metals, their reaction addition site, type of product (cycloaddition or single-bond adduct), and regioselectivity are different, confirming that the chemical properties of actinide EMFs are significantly different from those of lanthanide EMFs.

IV. EXPERIMENTAL SECTION

A. Materials and general instruments

U@C_{2v}(9)-C_{82} was synthesized using an improved arc-discharge method and separated by multi-stage HPLC procedures. A Buckyprep column (10 × 250 mm^2, Cosmosil, Nacalai Tesque, Japan) was employed with toluene as the eluent for high performance liquid chromatography (HPLC) separation. UV–vis–NIR spectra of the purified **2a** and **2b** were obtained with a Cary 5000 UV–vis–NIR spectrophotometer (Agilent, USA) in CS_2 solution. The positive-ion mode matrix assisted laser desorption/ionization time-of-flight (MALDI-TOF) spectrophotometer (Bruker, Germany) was employed for the mass characterization, with *trans*-2-[3-(4-tertbutylphenyl)-2-methyl-2-propenylidene] malononitrile as the matrix. Cyclic voltammetry (CV) was recorded in 1,2-dichlorobenzene (*o*-DCB) using a CHI-660E instrument. A conventional three-electrode cell consisting of a platinum counter electrode, a glassy carbon working electrode, and a silver reference electrode was used for the measurement. (n-Bu)$_4$NPF$_6$ (0.05 M) was used as a supporting electrolyte. The CV was measured at a scan rate of 100 mV s^{-1}.

B. Synthesis of U@C_{2v}(9)-C_{82}C(COOC_2H_5)$_2$

The reaction of U@C_{82} (3 mg, 2.5 μmol) with diethyl bromomalonate (0.75 μl, 4.4 μmol) was conducted at room temperature in the presence of 1,8-diazabicyclo[5.4.0]undec-7-ene (DBU) (0.2 μl, 1.3 μmol) in dry toluene under N_2. The reaction proceeded very readily over 2 h. The crude reaction mixture was filtered to remove a small amount of precipitate and separated by multistage separation on HPLC.

C. X-ray crystallographic study

The black block crystals of U@C_{2v}(9)-C_{82}C(COOC_2H_5)$_2$ · 2.6($C_{0.5}$S) · $C_{0.2}S_{0.3}$ were obtained by liquid–liquid bilayer diffusion methods of a solution of U@C_{2v}(9)-C_{82}C(COOC_2H_5)$_2$ in CS_2 and hexane as the poor solvent. X-ray data were collected at 123 K using a diffractometer (Bruker D8 Venture) equipped with a CCD collector. The multiscan method was used for absorption correction. The structures were solved using direct methods[67] and refined on F^2 using full matrix least-squares using the SHELXL2014 crystallographic software package.[68] Hydrogen atoms were inserted at calculated positions and constrained with isotropic thermal parameters.

Crystal data for U@C_{2v}(9)-C_{82}C(COOC_2H_5)$_2$ · 1.33(CS_2) · 0.17(CS): $C_{90.5}H_{10}O_4S_{2.83}U$, Mr = 1489.82, 0.08 × 0.06 × 0.04 mm^3, monoclinic, space group C 2/c (No. 15), a = 20.9887(17) Å, b = 20.9948(17) Å, c = 22.5877(18) Å, α = 90°, β = 101.237°(4), γ = 90°, V = 9762.5(14) $Å^3$, Z = 8, ρ_{calcd} = 2.027 g cm^{-3}, μ(Cu Kα) = 7.907 mm^{-1}, θ = 1.735–55.890°, T = 123(2) K, R_1 = 0.1286, and wR_2 = 0.3058 for all data; R_1 = 0.1062 and wR_1 = 0.2886 for 7208 reflections [I > 2.0σ(I)] with 1138 parameters. Goodness of fit indicator 1.019. Maximum residual electron density 1.352 e $Å^{-3}$. The crystallographic data for this structure have been deposited at the Cambridge Crystallographic Data Center (CCDC) with the deposition number 2466867.

D. Computational details

Geometry optimizations were performed with the Amsterdam Density Functional (ADF, v. 2019) software[69,70] by using the Kohn–Sham density functional theory (DFT). The PBE functional[71] in conjunction with the triple-ζ polarized (TZP) Slater-type orbital (STO) basis sets[72] was first used to optimize the structures of reactants, intermediates, transition states, and products. The scalar relativistic (SR) zero-order regular approximation (ZORA)[73] and the D3 dispersion corrections by Grimme were considered in the calculations.[74] The PBE optimized geometries of all the stationary points were re-optimized by using the PBE0 functional.[75] In addition, the PBE0 optimized geometries were recomputed as single-point energy calculations including solvent effects by means of the COnductor like Screening MOdel (COSMO), as implemented in ADF using toluene as a solvent.[76] The free-energy profiles of the selected intermediates, TS, and products were re-calculated using the Gaussian (G16) package[77] and the M06 functional[78] in combination with the polarizable continuum model (PCM)[79] to account for solvent effects (toluene), which was found to be a reliable methodology to study kinetic aspects of the Bingel–Hirsh reaction in endohedral metallofullerenes.[58,66] We used the 6-31g(d,p) basis set for lighter atoms[80–82] and the SDD basis for the U atom.[83]

SUPPLEMENTARY MATERIAL

See the supplementary material for additional details of experiments and computations.

ACKNOWLEDGMENTS

A.R.-F. and J.M.P. thank the Spanish Ministry of Science and Innovation (Grant No. PID2023-149905NB-I00 funded by MICIU/AEI/10.13039/501100011033 and by "ERDF/EU"), the Generalitat de Catalunya (Grant No. 2021SGR00110), and the URV for the support. N.C. thanks the National Science Foundation of China (Grant No. 52172051), the Natural Science Foundation of Jiangsu Province (Grant No. BK20200041), and the Priority Academic Program Development of Jiangsu Higher Education Institutions (PAPD). D.T. thanks the Spanish Ministry of Science and Innovation for a predoctoral fellowship.

AUTHOR DECLARATIONS

Conflict of Interest

The authors have no conflicts to disclose.

Author Contributions

Daniel Torrens: Investigation (lead); Writing – original draft (supporting). **Bei Li**: Investigation (lead); Writing – original draft (equal). **Qin Wang**: Investigation (lead); Writing – original draft

27 October 2025 16:00:08

© Author(s) 2025

(supporting). **Laura Abella**: Investigation (supporting); Supervision (supporting); Writing – original draft (supporting). **Yang-Rong Yao**: Data curation (equal); Supervision (lead); Writing – original draft (lead); Writing – review & editing (lead). **Josep M. Poblet**: Funding acquisition (equal); Supervision (equal); Writing – review & editing (equal). **Ning Chen**: Conceptualization (equal); Data curation (equal); Supervision (equal); Validation (equal); Writing – review & editing (equal). **Antonio Rodríguez-Fortea**: Conceptualization (equal); Data curation (equal); Funding acquisition (equal); Supervision (equal); Writing – original draft (equal); Writing – review & editing (equal).

DATA AVAILABILITY

The data that support the findings of this study are available within the article and its supplementary material as well as from the corresponding authors upon reasonable request.

REFERENCES

[1] A. A. Popov, S. Yang, and L. Dunsch, Chem. Rev. **113**, 5989–6113 (2013).
[2] S. Yang, T. Wei, and F. Jin, Chem. Soc. Rev. **46**, 5005–5058 (2017).
[3] Z. Hu, Y. Wang, A. Ullah, G. M. Gutiérrez-Finol, A. Bedoya-Pinto, P. Gargiani, D. Shi, S. Yang, Z. Shi, A. Gaita-Ariño, and E. Coronado, Chem **9**, 3613–3622 (2023).
[4] X. Li, M. Zhen, R. Deng, T. Yu, J. Li, Y. Zhang, T. Zou, Y. Zhou, Z. Lu, M. Guan, H. Xu, C. Shu, and C. Wang, Biomaterials **163**, 142–153 (2018).
[5] J. Qiu, L. Abella, X. Du, Z. Cao, Z. He, Q. Meng, Y. Yan, J. M. Poblet, L. Sun, A. Rodríguez-Fortea, and N. Chen, J. Am. Chem. Soc. **146**, 24310–24319 (2024).
[6] Y. Wang, G. Velkos, N. J. Israel, M. Rosenkranz, B. Büchner, F. Liu, and A. A. Popov, J. Am. Chem. Soc. **143**, 18139–18149 (2021).
[7] B. Wu, T. Wang, Y. Feng, Z. Zhang, L. Jiang, and C. Wang, Nat. Commun. **6**, 6468 (2015).
[8] K. Zhang, C. Wang, M. Zhang, Z. Bai, F.-F. Xie, Y.-Z. Tan, Y. Guo, K.-J. Hu, L. Cao, S. Zhang, X. Tu, D. Pan, L. Kang, J. Chen, P. Wu, X. Wang, J. Wang, J. Liu, Y. Song, G. Wang, F. Song, W. Ji, S.-Y. Xie, S.-F. Shi, M. A. Reed, and B. Wang, Nat. Nanotechnol. **15**, 1019–1024 (2020).
[9] Y. Zhou, R. Deng, M. Zhen, J. Li, M. Guan, W. Jia, X. Li, Y. Zhang, T. Yu, T. Zou, Z. Lu, J. Guo, L. Sun, C. Shu, and C. Wang, Biomaterials **133**, 107–118 (2017).
[10] F. Liu, D. S. Krylov, L. Spree, S. M. Avdoshenko, N. A. Samoylova, M. Rosenkranz, A. Kostanyan, T. Greber, A. U. B. Wolter, B. Büchner, and A. A. Popov, Nat. Commun. **8**, 16098 (2017).
[11] F. Liu, G. Velkos, D. S. Krylov, L. Spree, M. Zalibera, R. Ray, N. A. Samoylova, C.-H. Chen, M. Rosenkranz, S. Schiemenz, F. Ziegs, K. Nenkov, A. Kostanyan, T. Greber, A. U. B. Wolter, M. Richter, B. Büchner, S. M. Avdoshenko, and A. A. Popov, Nat. Commun. **10**, 571 (2019).
[12] G. Velkos, D. S. Krylov, K. Kirkpatrick, L. Spree, V. Dubrovin, B. Büchner, S. M. Avdoshenko, V. Bezmelnitsyn, S. Davis, P. Faust, J. Duchamp, H. C. Dorn, and A. A. Popov, Angew. Chem., Int. Ed. **58**, 5891–5896 (2019).
[13] Y. Chai, T. Guo, C. Jin, R. E. Haufler, L. P. F. Chibante, J. Fure, L. Wang, J. M. Alford, and R. E. Smalley, J. Phys. Chem. **95**, 7564–7568 (1991).
[14] A. Rodriguez-Fortea, N. Alegret, A. L. Balch, and J. M. Poblet, Nat. Chem. **2**, 955–961 (2010).
[15] A. Rodríguez-Fortea, A. L. Balch, and J. M. Poblet, Chem. Soc. Rev. **40**, 3551–3563 (2011).
[16] S. Stevenson, G. Rice, T. Glass, K. Harich, F. Cromer, M. R. Jordan, J. Craft, E. Hadju, R. Bible, M. M. Olmstead, K. Maitra, A. J. Fisher, A. L. Balch, and H. C. Dorn, Nature **401**, 55–57 (1999).
[17] W. Cai, L. Abella, J. Zhuang, X. Zhang, L. Feng, Y. Wang, R. Morales-Martínez, R. Esper, M. Boero, A. Metta-Magaña, A. Rodríguez-Fortea, J. M. Poblet, L. Echegoyen, and N. Chen, J. Am. Chem. Soc. **140**, 18039–18050 (2018).
[18] W. Cai, R. Morales-Martinez, X. Zhang, D. Najera, E. L. Romero, A. Metta-Magana, A. Rodriguez-Fortea, S. Fortier, N. Chen, J. M. Poblet, and L. Echegoyen, Chem. Sci. **8**, 5282–5290 (2017).
[19] Q. Meng, R. Morales-Martinez, J. Zhuang, Y.-R. Yao, Y. Wang, L. Feng, J. M. Poblet, A. Rodriguez-Fortea, and N. Chen, Inorg. Chem. **60**, 11496–11502 (2021).
[20] Y. Wang, R. Morales-Martinez, X. Zhan, W. Yang, Y. Wang, A. Rodriguez-Fortea, J. M. Poblet, L. Feng, S. Wang, and N. Chen, J. Am. Chem. Soc. **139**, 5110–5116 (2017).
[21] Y.-R. Yao, Y. Roselló, L. Ma, A. R. P. Santiago, A. Metta-Magaña, N. Chen, A. Rodriguez-Fortea, J. M. Poblet, and L. Echegoyen, J. Am. Chem. Soc. **143**, 15309–15318 (2021).
[22] A. Moreno-Vicente, M. Alias-Rodriguez, P. W. Dunk, C. de Graaf, J. M. Poblet, and A. Rodriguez-Fortea, Inorg. Chem. Front. **10**, 908–914 (2023).
[23] A. Moreno-Vicente, Y. Rosello, N. Chen, L. Echegoyen, P. W. Dunk, A. Rodriguez-Fortea, C. de Graaf, and J. M. Poblet, J. Am. Chem. Soc. **145**, 6710–6718 (2023).
[24] Y. Yan, L. Abella, R. Sun, Y.-H. Fang, Y. Rosello, Y. Shen, M. Jin, A. Rodriguez-Fortea, C. de Graaf, Q. Meng, Y.-R. Yao, L. Echegoyen, B.-W. Wang, S. Gao, J. M. Poblet, and N. Chen, Nat. Commun. **14**, 6637 (2023).
[25] X. Zhang, Y. Wang, R. Morales-Martinez, J. Zhong, C. de Graaf, A. Rodriguez-Fortea, J. M. Poblet, L. Echegoyen, L. Feng, and N. Chen, J. Am. Chem. Soc. **140**, 3907–3915 (2018).
[26] J. Zhuang, R. Morales-Martinez, J. Zhang, Y. Wang, Y.-R. Yao, C. Pei, A. Rodriguez-Fortea, S. Wang, L. Echegoyen, C. de Graaf, J. M. Poblet, and N. Chen, Nat. Commun. **12**, 2372 (2021).
[27] Y. Shen, Y. Rosello, L. Abella, J. Qiu, X. Du, Q. Meng, L. Zheng, Z. Cao, Z. He, J. M. Poblet, L. Echegoyen, L. Sun, A. Rodriguez-Fortea, and N. Chen, J. Am. Chem. Soc. **146**, 34924–34933 (2024).
[28] F. Liu, L. Spree, D. S. Krylov, G. Velkos, S. M. Avdoshenko, and A. A. Popov, Acc. Chem. Res. **52**, 2981–2993 (2019).
[29] X. Li, Y. Rosello, Y.-R. Yao, J. Zhuang, X. Zhang, A. Rodriguez-Fortea, C. de Graaf, L. Echegoyen, J. M. Poblet, and N. Chen, Chem. Sci. **12**, 282–292 (2021).
[30] Y. Shen, X. Yu, Q. Meng, Y.-R. Yao, J. Autschbach, and N. Chen, Chem. Sci. **13**, 12980–12986 (2022).
[31] X. Zhang, W. Li, L. Feng, X. Chen, A. Hansen, S. Grimme, S. Fortier, D.-C. Sergentu, T. J. Duignan, J. Autschbach, S. Wang, Y. Wang, G. Velkos, A. A. Popov, N. Aghdassi, S. Duhm, X. Li, J. Li, L. Echegoyen, W. H. E. Schwarz, and N. Chen, Nat. Commun. **9**, 2753 (2018).
[32] J. Zhuang, L. Abella, D.-C. Sergentu, Y.-R. Yao, M. Jin, W. Yang, X. Zhang, X. Li, D. Zhang, Y. Zhao, X. Li, S. Wang, L. Echegoyen, J. Autschbach, and N. Chen, J. Am. Chem. Soc. **141**, 20249–20260 (2019).
[33] R. D. Bolskar, A. F. Benedetto, L. O. Husebo, R. E. Price, E. F. Jackson, S. Wallace, L. J. Wilson, and J. M. Alford, J. Am. Chem. Soc. **125**, 5471–5478 (2003).
[34] Y. Li, R. Biswas, W. P. Kopcha, T. Dubroca, L. Abella, Y. Sun, R. A. Crichton, C. Rathnam, L. Yang, Y.-W. Yeh, K. Kundu, A. Rodríguez-Fortea, J. M. Poblet, K.-B. Lee, S. Hill, and J. Zhang, Angew. Chem., Int. Ed. **62**, e202211704 (2023).
[35] J. Zhang, Y. Ye, Y. Chen, C. Pregot, T. Li, S. Balasubramaniam, D. B. Hobart, Y. Zhang, S. Wi, R. M. Davis, L. A. Madsen, J. R. Morris, S. M. LaConte, G. T. Yee, and H. C. Dorn, J. Am. Chem. Soc. **136**, 2630–2636 (2014).
[36] Z. Ge, J. C. Duchamp, T. Cai, H. W. Gibson, and H. C. Dorn, J. Am. Chem. Soc. **127**, 16292–16298 (2005).
[37] S. Stevenson, K. Harich, H. Yu, R. R. Stephen, D. Heaps, C. Coumbe, and J. P. Phillips, J. Am. Chem. Soc. **128**, 8829–8835 (2006).
[38] Y. Sun, L. Abella, T. J. Emge, S. Zhu, Y. Li, I. Ferraro, A. Li, S. Stevenson, J. M. Poblet, A. Rodríguez-Fortea, and J. Zhang, Angew. Chem., Int. Ed. **64**, e202424776 (2025).
[39] C. M. Cardona, A. Kitaygorodskiy, and L. Echegoyen, J. Am. Chem. Soc. **127**, 10448–10453 (2005).
[40] O. Lukoyanova, C. M. Cardona, J. Rivera, L. Z. Lugo-Morales, C. J. Chancellor, M. M. Olmstead, A. Rodríguez-Fortea, J. M. Poblet, A. L. Balch, and L. Echegoyen, J. Am. Chem. Soc. **129**, 10423–10430 (2007).
[41] S. Aroua and Y. Yamakoshi, J. Am. Chem. Soc. **134**, 20242–20245 (2012).

27 October 2025 16:00:08

© Author(s) 2025

[42]T. Cai, C. Slebodnick, L. Xu, K. Harich, T. E. Glass, C. Chancellor, J. C. Fettinger, M. M. Olmstead, A. L. Balch, H. W. Gibson, and H. C. Dorn, J. Am. Chem. Soc. **128**, 6486–6492 (2006).
[43]E. B. Iezzi, J. C. Duchamp, K. Harich, T. E. Glass, H. M. Lee, M. M. Olmstead, A. L. Balch, and H. C. Dorn, J. Am. Chem. Soc. **124**, 524–525 (2002).
[44]H. M. Lee, M. M. Olmstead, E. Iezzi, J. C. Duchamp, H. C. Dorn, and A. L. Balch, J. Am. Chem. Soc. **124**, 3494–3495 (2002).
[45]S. Stevenson, R. R. Stephen, T. M. Amos, V. R. Cadorette, J. E. Reid, and J. P. Phillips, J. Am. Chem. Soc. **127**, 12776–12777 (2005).
[46]Y. Hu, Y.-R. Yao, X. Liu, A. Yu, X. Xie, L. Abella, A. Rodríguez-Fortea, J. M. Poblet, T. Akasaka, P. Peng, Q. Zhang, S.-Y. Xie, F.-F. Li, and X. Lu, Chem. Sci. **12**, 8123–8130 (2021).
[47]Y. Iiduka, O. Ikenaga, A. Sakuraba, T. Wakahara, T. Tsuchiya, Y. Maeda, T. Nakahodo, T. Akasaka, M. Kako, N. Mizorogi, and S. Nagase, J. Am. Chem. Soc. **127**, 9956–9957 (2005).
[48]C. Shu, C. Slebodnick, L. Xu, H. Champion, T. Fuhrer, T. Cai, J. E. Reid, W. Fu, K. Harich, H. C. Dorn, and H. W. Gibson, J. Am. Chem. Soc. **130**, 17755–17760 (2008).
[49]C. Shu, T. Cai, L. Xu, T. Zuo, J. Reid, K. Harich, H. C. Dorn, and H. W. Gibson, J. Am. Chem. Soc. **129**, 15710–15717 (2007).
[50]T. Wakahara, Y. Iiduka, O. Ikenaga, T. Nakahodo, A. Sakuraba, T. Tsuchiya, Y. Maeda, M. Kako, T. Akasaka, K. Yoza, E. Horn, N. Mizorogi, and S. Nagase, J. Am. Chem. Soc. **128**, 9919–9925 (2006).
[51]M. Yamada, T. Abe, C. Saito, T. Yamazaki, S. Sato, N. Mizorogi, Z. Slanina, F. Uhlík, M. Suzuki, Y. Maeda, Y. Lian, X. Lu, M. M. Olmstead, A. L. Balch, S. Nagase, and T. Akasaka, Chem. - Eur. J. **23**, 6552–6561 (2017).
[52]S. Yang, X. Zhou, Y. Hu, L. Abella, Y.-R. Yao, P. Peng, Q. Zhang, A. Rodríguez-Fortea, J. M. Poblet, and F.-F. Li, J. Org. Chem. **88**, 4234–4243 (2023).
[53]X. Liu, B. Li, W. Yang, Y.-R. Yao, L. Yang, J. Zhuang, X. Li, P. Jin, and N. Chen, Chem. Sci. **12**, 2488–2497 (2021).
[54]Q. Wang, L. Abella, Y.-R. Yao, Y. Yan, D. Torrens, Q. Meng, S. Yang, J. M. Poblet, A. Rodríguez-Fortea, and N. Chen, Inorg. Chem. **62**, 12976–12988 (2023).
[55]L. Feng, T. Nakahodo, T. Wakahara, T. Tsuchiya, Y. Maeda, T. Akasaka, T. Kato, E. Horn, K. Yoza, N. Mizorogi, and S. Nagase, J. Am. Chem. Soc. **127**, 17136–17137 (2005).
[56]L. Feng, T. Wakahara, T. Nakahodo, T. Tsuchiya, Q. Piao, Y. Maeda, Y. Lian, T. Akasaka, E. Horn, K. Yoza, T. Kato, N. Mizorogi, and S. Nagase, Chem. - Eur. J. **12**, 5578–5586 (2006).
[57]C. Bingel, Chem. Ber. **126**, 1957–1959 (1993).
[58]N. Alegret, A. Rodriguez-Fortea, and J. M. Poblet, Chem. Eur. J. **19**, 5061–5069 (2013).
[59]M. Garcia-Borràs, M. R. Cerón, S. Osuna, M. Izquierdo, J. M. Luis, L. Echegoyen, and M. Solà, Angew. Chem., Int. Ed. **55**, 2374–2377 (2016).
[60]R. He, H. Zhao, J. Liu, Y. Jiao, Y. Liang, X. Li, and C. Chen, Fullerenes, Nanotubes Carbon Nanostruct. **21**, 549–559 (2013).
[61]W. Shen, L. Yang, B. Li, P. Jin, B. Yu, H. Cong, T. Akasaka, and X. Lu, Chem. Commun. **56**, 14357–14360 (2020).
[62]Q.-Z. Li, J.-J. Zheng, and X. Zhao, J. Phys. Chem. C **119**, 26196–26201 (2015).
[63]J. Pablo Martinez, M. Garcia-Borras, S. Osuna, J. Poater, F. Matthias Bickelhaupt, and M. Sola, Chem. Eur. J. **22**, 5953–5962 (2016).
[64]N. Alegret, M. N. Chaur, E. Santos, A. Rodríguez-Fortea, L. Echegoyen, and J. M. Poblet, J. Org. Chem. **75**, 8299–8302 (2010).
[65]M. Garcia-Borràs, S. Osuna, M. Swart, J. M. Luis, L. Echegoyen, and M. Solà, Chem. Commun. **49**, 8767–8769 (2013).
[66]N. Alegret, P. Salvado, A. Rodriguez-Fortea, and J. M. Poblet, J. Org. Chem. **78**, 9986–9990 (2013).
[67]O. V. Dolomanov, L. J. Bourhis, R. J. Gildea, J. A. K. Howard, and H. Puschmann, J. Appl. Crystallogr. **42**, 339–341 (2009).
[68]G. M. Sheldrick, Acta Crystallogr., Sect. C: Struct. Chem. **71**, 3–8 (2015).
[69]ADF, Theoretical Chemistry, Vrije Universiteit, Amsterdam, The Netherlands, 2019, http://www.scm.com.
[70]G. te Velde, F. M. Bickelhaupt, E. J. Baerends, C. Fonseca Guerra, S. J. A. Van Gisbergen, J. G. Snijders, and T. Ziegler, J. Comput. Chem. **22**, 931–967 (2001).
[71]J. P. Perdew, K. Burke, and M. Ernzerhof, Phys. Rev. Lett. **77**, 3865–3868 (1996).
[72]E. Van Lenthe and E. J. Baerends, J. Comput. Chem. **24**, 1142–1156 (2003).
[73]E. v. Lenthe, E. J. Baerends, and J. G. Snijders, J. Chem. Phys. **99**, 4597–4610 (1993).
[74]S. Grimme, S. Ehrlich, and L. Goerigk, J. Comput. Chem. **32**, 1456–1465 (2011).
[75]C. Adamo and V. Barone, J. Chem. Phys. **110**, 6158–6170 (1999).
[76]A. Klamt, J. Phys. Chem. **99**, 2224–2235 (1995).
[77]M. J. Frisch, G. W. Trucks, H. B. Schlegel, G. E. Scuseria, M. A. Robb, J. R. Cheeseman, G. Scalmani, V. Barone, G. A. Petersson, H. Nakatsuji, X. Li, M. Caricato, A. V. Marenich, J. Bloino, B. G. Janesko, R. Gomperts, B. Mennucci, H. P. Hratchian, J. V. Ortiz, A. F. Izmaylov, J. L. Sonnenberg, Williams, F. Ding, F. Lipparini, F. Egidi, J. Goings, B. Peng, A. Petrone, T. Henderson, D. Ranasinghe, V. G. Zakrzewski, J. Gao, N. Rega, G. Zheng, W. Liang, M. Hada, M. Ehara, K. Toyota, R. Fukuda, J. Hasegawa, M. Ishida, T. Nakajima, Y. Honda, O. Kitao, H. Nakai, T. Vreven, K. Throssell, J. A. Montgomery, Jr., J. E. Peralta, F. Ogliaro, M. J. Bearpark, J. J. Heyd, E. N. Brothers, K. N. Kudin, V. N. Staroverov, T. A. Keith, R. Kobayashi, J. Normand, K. Raghavachari, A. P. Rendell, J. C. Burant, S. S. Iyengar, J. Tomasi, M. Cossi, J. M. Millam, M. Klene, C. Adamo, R. Cammi, J. W. Ochterski, R. L. Martin, K. Morokuma, O. Farkas, J. B. Foresman, and D. J. Fox, Gaussian 16, Revision C.01, Wallingford, CT, 2016.
[78]Y. Zhao and D. G. Truhlar, Theor. Chem. Acc. **120**, 215–241 (2008).
[79]J. Tomasi, B. Mennucci, and R. Cammi, Chem. Rev. **105**, 2999–3094 (2005).
[80]P. C. Hariharan and J. A. Pople, Theor. Chim. Acta **28**, 213–222 (1973).
[81]W. J. Hehre, R. Ditchfield, and J. A. Pople, J. Chem. Phys. **56**, 2257 (1972).
[82]V. A. Rassolov, M. A. Ratner, J. A. Pople, P. C. Redfern, and L. A. Curtiss, J. Comput. Chem. **22**, 976–984 (2001).
[83]M. Dolg and X. Cao, J. Phys. Chem. A **113**, 12573–12581 (2009).

27 October 2025 16:00:08

© Author(s) 2025